Available online at www.sciencedirect.com
ScienceDirect
Ceramics International 36 (2010) 1961–1969
CERAMICS INTERNATIONAL
www.elsevier.com/locate/ceramint

Synthesis of nanocrystalline hydroxyapatite from $Ca(OH)_2$ and H_3PO_4 assisted by ultrasonic irradiation

Marina A. Giardina, María A. Fanovich *

Institute of Materials Science and Technology (INTEMA), University of Mar del Plata and National Research Council (CONICET), J. B. Justo 4302, 7600 Mar del Plata, Argentina

Received 18 January 2010; received in revised form 6 February 2010; accepted 16 April 2010
Available online 11 June 2010

Abstract

This work is focused on the synthesis of hydroxyapatite powders by precipitation assisted by a tip ultrasonic irradiation (UI) from $Ca(OH)_2$ and H_3PO_4. The effect of UI time, applied UI power during the synthesis, initial Ca^{2+} concentration and ageing time of the mixture on phase composition, morphology and specific surface area of the obtained powders was analysed. Particles obtained from the precipitation method using UI or mechanical agitation were compared with a nanosized hydroxyapatite of reference in terms of crystal size, phase composition and thermal stability. This study revealed the feasibility to produce hydroxyapatite powders with controlled crystal size between 31.7 and 70.6 nm by ultrasonic assisted precipitation method. Hydroxyapatite powder with similar surface area to the reference material can be obtained adjusting experimental conditions. The used method allowed us to synthesise hydroxyapatite powders with thermal stability up to 1100 °C.

Keywords: A. Powders: chemical preparation; D. Apatite; E. Biomedical applications

1. Introduction

Hydroxyapatite ($Ca_{10}(PO_4)_6(OH)_2$, HA) is used as a biomaterial for the regeneration of bone tissue because its chemical and crystallographic similarities with the main inorganic component of natural bone [1,2]. Over the past several decades, HA has attracted much attention as a substitute material for damaged teeth or bones because it has excellent properties such as biocompatibility, osteoconductivity and bioactivity. These characteristics promote the use of HA powders in different composite materials with the objective of increasing the degree of bioactivity and thus enhancing the performance of the developed new materials [3,4].

Another relevant property of HA is its ability to adsorb different chemical species on the surface. This property has been exploited in different clinical requirements of various applications. Moreover, the great affinity of HA for various active molecules can be used for the development of drug delivery devices [5–7].

Many methods have been reported for synthesising HA including solid-state reaction, precipitation methods, sol–gel, hydrothermal, electrophoretic deposition methods among others [8–12]. The product characteristics are highly influenced by the variables of synthesis. Depending upon the technique, materials with different morphology, stoichiometry, and level of crystallinity can be obtained [13,14].

The precipitation process is the most reported method for preparing HA materials. This process is simple, low cost and suitable for industrial production but the product is generally obtained as large size crystalline particles or agglomerates of nanoparticles. Further, when a calcium phosphate material is precipitated, the used molar ratio Ca/P, the synthesis temperature, the method of agitation, the pH of the reaction mixture, the rate of adding the reagents, the ageing time, etc. are variables that affect the final characteristics of the precipitated powder [15,16].

For specific biomedical applications it is necessary to produce HA crystallites with reduced particle sizes and high surface areas, or controlled morphology, or both. Current studies are directed to investigate different routes of synthesis for obtaining HA nanopowders [17–19] in order to achieve a bioactive phase that can be used in combination with other

* Corresponding author.
E-mail address: mafanovi@fi.mdp.edu.ar (M.A. Fanovich).

0272-8842/$36.00
doi:10.1016/j.ceramint.2010.05.008

materials that lack this property [20] and thus to produce nanostructured composite materials.

On the other hand, recent investigations reveal that the reactivity of chemical species in solution being involved in a synthesis process can be stimulated by ultrasonic irradiation (UI) of the reaction mixture. It has been recognised that this type of treatment causes cavitation in an aqueous medium inducing formation, growth and collapse of micro bubbles. This intense agitation process leads to events of dissolution–precipitation of solids through which a reduction of particle size and surface activation of solid materials is produced [21–23]. The efficiency of the synthesis process depends on many variables especially taking into account the type of used ultrasonic device, e.g. the use of a tip ultrasonic homogenizer is more efficient than an ultrasonic bath.

In this work, the synthesis of HA powders has been studied by precipitation assisted by a tip ultrasonic irradiation (UI) of $Ca(OH)_2$ and H_3PO_4 with the purpose of obtaining HA particles with a high specific surface that can be used as OH^-- or CO_3^{2-}-activated surface for producing nanostructured biomaterials. The effect of UI time, applied UI power during the synthesis, initial Ca^{2+} concentration and ageing time of the mixture on phase composition, morphology and specific surface area of the obtained powders was analysed. Particles obtained from the precipitation method using UI or mechanical agitation were compared with a nanosized hydroxyapatite of reference in terms of crystal size, phase composition and thermal stability [24].

2. Materials and methods

The starting materials used in this work were analytical grade: $CaCO_3$ (99%, PA Cicarelli) as the Ca source and H_3PO_4 (85%, Merck) as the P source. The $CaCO_3$ was thermally treated in an oven (Indef, model 332 p-full) at 1200 °C for 2 h to obtain CaO. The flow chart of the synthesis is depicted in Fig. 1. Two methods of agitation were used, conventional mechanical stirring (MS) and ultrasound (IU) using a commercially available device (Sonics vibra-cell, VCX130, USA) that produces acoustic waves at a frequency of 60 kHz with a maximum power of 130 W. The CaO solid was first dispersed in ammonium hydroxide (pH = 12) and then treated by MS or IU during different times (t_1). Subsequently, 10 mL of H_3PO_4 0.5 mol/L was slowly added dropwise into the same beaker at 2 mL/min until reaching a molar ratio of Ca/P ~1.67 (t_2). After this step, the reaction mixture was MS or IU treated (t_3) and then kept at an ageing step (t_4). An additional application of UI was applied (t_5) after ageing in one synthesis. All steps were carried out at room temperature (~25 °C). The pH of the suspension was measured before and after of the precipitation process. Finally, the precipitate was centrifuged and freeze-dried. Ten samples were obtained following the described process. Detailed information for each prepared powder is given in Table 1. A nano-HA powder (R-HA), obtained by the López Macipe method, was used as reference material for characterisation [24].

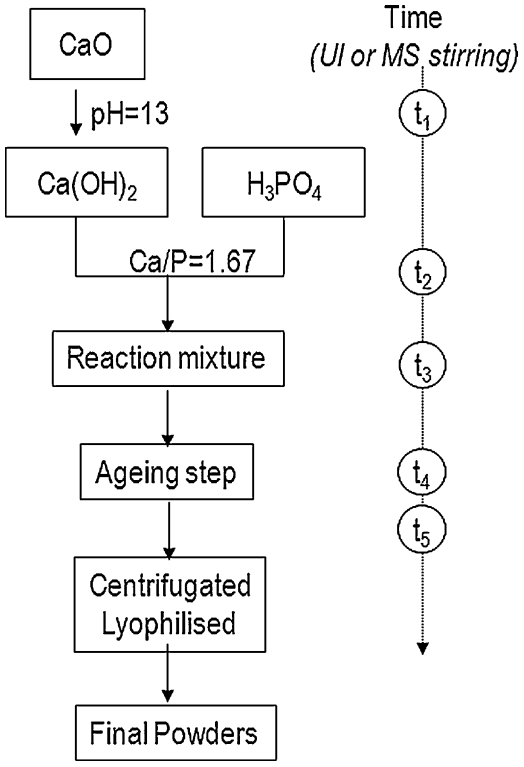

Fig. 1. Flow chart of the synthesis method.

The obtained powders were characterised by X-ray powder diffraction (XRD, Philips 1830/00) with Ni-filtered Cu-K_α radiation (λ = 1.54050 Å). The electrical voltage and current were 40 kV and 30 mA, respectively. Data were collected for 2θ ranging between 10° and 70° with a step size of 1°/min. Crystal sizes (D) of the synthesised HA powders were determined with the aid of Scherrer equation. To assess the instrumental line broadening, the XRD pattern of a standard microcrystalline silicon powder was recorded.

$$D = \frac{0.9\lambda}{B\cos\theta_B} \quad (1)$$

where

$$B = (b^2 - \beta^2)^{1/2} \quad (2)$$

and b = experimental line broadening, β = instrumental line broadening.

The specific surface area (SSA) of dried powders was measured by gas adsorption in N_2 atmosphere (BET method) with a Micromeritics Flowsorb II 2300 device.

Fourier-transformed infrared (FTIR) spectra were recorded with a Genesis II-Mattson device in the absorbance mode, in the range 400–4000 cm^{-1} with a resolution of 2 cm^{-1}. Spectra were obtained using pellets of the powders with KBr.

The powder morphologies were evaluated by using scanning electron microscopy (SEM, Jeol JXA-8600). Samples were gold coated and examined at 10–15 kV.

Finally, the UI-synthesised powders were treated in an electric oven at 200, 600 and 1100 °C, during 2 h. Then, the

Table 1
Synthesis conditions of the obtained powders.

	Sample	Agitation	t_1 (min)	t_2 (min)	t_3 (min)	t_4 (h)	t_5 (min)	Power	[Ca^{2+}] M
G1-Group	S1	MS	3	1	3	0	–	1000 rpm	0.1
	S2	UI	3	1	3	0	–	65 W	0.1
	S3	MS	3	1	3	24	–	1000 rpm	0.1
	S4	UI	3	1	3	24	–	65 W	0.1
	S5	MS	3	1	3	48	–	1000 rpm	0.1
	S6	UI	3	1	3	48	–	65 W	0.1
G2-Group	S7	UI	6	1	6	48	–	65 W	0.1
	S8	UI	3	1	3	48	3 min	65 W	0.1
	S9	UI	3	1	3	48	–	130 W	0.1
	S10	UI	3	1	3	48	–	65 W	0.02
	R-HA	Nanosized hydroxyapatite of Ref. [24]							0.02

calcined samples were characterised by XRD and crystal sizes (D) to evaluate their thermal stability.

3. Results and discussion

Fig. 2 shows the XRD patterns of G1-Group after freeze-drying. Two crystalline phases are detected in S1, S2, S3 and S5 samples, one is HA and the other is $Ca(OH)_2$. The S4 and S6 samples are only formed by a HA phase; the peak intensity of $Ca(OH)_2$ is not detected in these samples obtained using UI and 24 or 48 h of ageing time. The main indices (*h k l*) for HA and $Ca(OH)_2$ are indicated on the spectra according to the International Centre for Diffraction Data. This result shows that the ultrasound irradiation is very effective to obtain HA as main phase when the precipitates are at least aged for 24 h. The ageing step favours HA formation from activated precursors by UI. In these syntheses we observed that the key factor is a synergistic effect of UI and the ageing step. The treatment with ultrasonic irradiation stimulates the reactivity of chemical species involved, resulting in the acceleration of the heterogeneous reactions between liquid and solid reactants in the period of ageing.

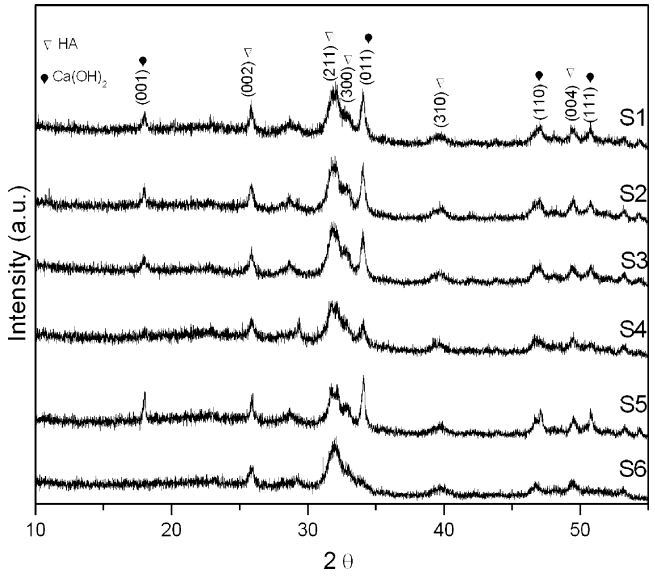

Fig. 2. XRD patterns of G1-Group of samples.

Kim and Cho studied the sonochemical synthesis of HA from H_3PO_4 and $Ca(OH)_2$ [25]. They assume that, at the initial stage of reaction (between 5 and 15 min), the predominant reaction is the formation of $CaHPO_4{\cdot}2H_2O$ (DCPD) and describe the formation of DCPD as an intermediate that occurs as a typical acid–base reaction. In the system investigated here, this intermediate should be detected in the S2 sample (without ageing). However, this phase is not identified due to the differing conditions used. Probably, the DCPD phase is not formed due to the elevated initial pH value of the suspension that favours the direct formation of HA with MS or UI, calcium phosphate being more basic than DCPD, according to the following reaction:

$$6H_3PO_4 + 10Ca(OH)_2 \rightarrow Ca_{10}(PO_4)_6(OH)_2 + 18H_2O \quad (3)$$

In all syntheses, variations in the pH of the suspension before and after precipitation were not significant due to the excess of ammonium hydroxide in the mixture of reaction (pH ∼12). However, the pH values of the suspensions decreased in samples after the ageing period, where the values range from 10 to 11. This fact agrees with the known process of HA formation via wet synthesis.

The direct precipitation of HA depends on the availability of PO_4^{3-}, Ca^{2+} and OH^- ions in the solution, being the agitation method a key factor to facilitate the dissolution processes of solids.

Increasing of the temperature up to 80 °C in the UI assisted syntheses, an effect associated with the UI application, favours the dissolution events in the reaction mixture. Consequently, the UI treatment resulted in a method more efficient than the mechanical stirring to produce HA monophase powders, as can be observed in the S4 and S6 sample compositions.

Fig. 3 shows the XRD patterns of four samples (G2-Group) obtained by employing UI treatment in the synthesis varying the UI time (S7), with UI additional treatment (S8), the UI power (S9) and the initial calcium ion concentration (S10). These set of samples showed a significant decrease in the pH

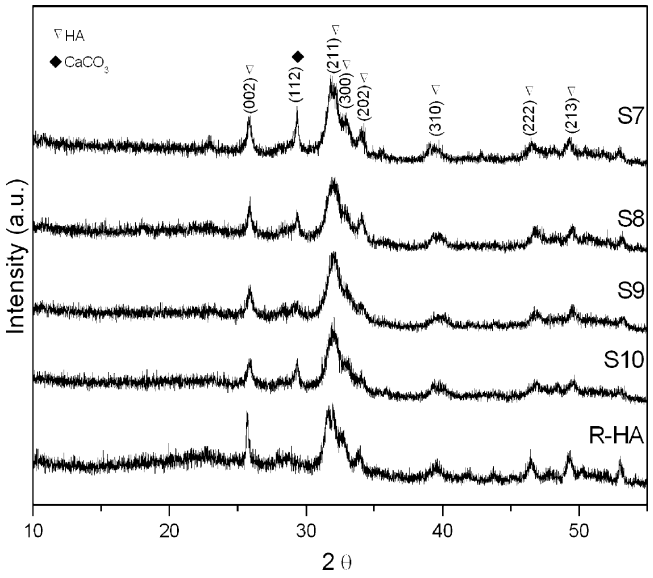

Fig. 3. XRD patterns of G2-Group of samples.

suspension after the ageing period from ~13 to ~9–10. Also, these powders showed the formation of HA phase differing slightly in the HA diffraction peak intensities. No characteristic peaks of $Ca(OH)_2$ phase can be seen in the spectra of G2-Group. The observed peak at $2\theta = 29.1$ in Fig. 3 is assigned to $CaCO_3$ phase that is present in the S7 sample and with minor intensity in S8 and S10. During ultrasonic irradiation, $CaCO_3$ is formed from $Ca(OH)_2$ by absorbing atmospheric CO_2 in the mentioned samples. The formation of $CaCO_3$ in some samples is an evidence of the major reactivity of remnant $Ca(OH)_2$ of the reaction. The presence of CO_3^{2-} in the HA structure cannot be determined from the results of the XRD spectra. The high power of UI employed in the S9-synthesis favoured the formation of pure HA phase. XRD spectrum of R-HA shows the typical signals of hydroxyapatite with low crystallinity similar in appearance to the XRD of synthesised samples. However, the reference powder does not exhibit secondary phases.

All synthesised powders showed wide and high peaks in the XRD spectra, indicating that the crystal sizes are very small with good crystallinity. The crystal sizes D of the samples were determined by Eq. (1) in nanometers. The peaks assigned to (0 0 2) plane were chosen for calculating the crystallite size as shown in Table 2. The contribution to the peak breadth from instrumental broadening was determined to be 1.6×10^{-3} rad. The *D* values obtained for G1-Group resulted roughly two-fold larger than that calculated for G2-Group, except for S6. This significant difference was fundamentally assigned to the effect of time and power of UI treatment. This stage consists in a series of dynamic processes where the dissolution and re-precipitation of solids take place, resulting in powders with minor crystal sizes than the ones obtained by using MS (to compare S2 with S6 and S1 with S5 crystal sizes). Nanocrystalline HA powders can be obtained adjusting the reaction conditions and using reduced time periods of UI treatment (7–10 min) compared with those reported in the literature (60 min).

Fig. 4 shows the FTIR spectra recorded for all synthesised powders. The bands at 1100 and 1035 cm^{-1} are due to the υ_3 mode (stretching vibration) of the phosphate group. The peak at 469 cm^{-1} is assigned to the υ_2 phosphate mode (bending vibration) and the bands at 563 and 600 cm^{-1} are due to the υ_4 phosphate mode (bending vibration). The spectra also show the υ_1 PO_4^{3-} mode peaks at 963 cm^{-1} due to stretching vibration. The band at 1635 cm^{-1} is due to H_2O bending mode and a broad peak at 3450 cm^{-1} indicates the adsorbed water. The characteristic peaks at 3572 cm^{-1} due to υ_s (OH) and 650 cm^{-1} due to υ_l (OH) in the hydroxyapatite lattice are almost imperceptible in the spectra. However, this does not mean that OH is not present in the HA structure. Taylor et al. [26] have reported that infrared spectra are not definitive for determining the OH presence in HA structure, due to the fact that the libration band is often concealed by the broadening of the phosphate bands particularly in poorly crystalline materials. They solved this difficulty carrying out other spectra using high energy transfer inelastic neutron scattering spectroscopy.

In our spectra the peak at 3637 cm^{-1} is assigned to the OH stretching in $Ca(OH)_2$ [27–29].

Moreover, the characteristic bands for the CO_3^{2-} group occur in the spectral regions 1400–1600 cm^{-1} (υ_3, asymmetric stretch vibration) and 873–880 cm^{-1} (υ_2, out-of-plane bend vibration). CO_3^{2-} incorporation in synthetic HA has been classified as either type A or type B depending on the mode of CO_3^{2-} substitution. When CO_3^{2-} replaces HO^-, the substitution is named type A, while in that case when CO_3^{2-} replaces PO_4^{3-}, the substitution is named type B. Non-specific substitution is represented as CO_3-HA (carbonate hydroxyapatite).

In this study, the bands associated to CO_3^{2-} result from overlapping of bands of $CaCO_3$ and probably of CO_3-HA. It is not possible to confirm a type of CO_3^{2-} substitution in all synthesised samples due to the presence of $CaCO_3$ crystals (Calcite) detected by XRD in some samples. However, it is possible to affirm that CO_3^{2-} ions are present in the structure of HA in the samples S6 and S9. The R-HA sample shows characteristic bands of PO_4^{3-} and COO^- groups (symmetric

Table 2
Crystal sizes (*D*, nm) determined by Scherrer equation on synthesised powders.

	Sample										
	G1-Group							G2-Group			
	S1	S2	S3	S4	S5	S6	S7	S8	S9	S10	R-HA
D (nm)	70.6	67.5	70.6	59.7	70.6	41.2	31.7	32.3	33.0	31.7	25.2

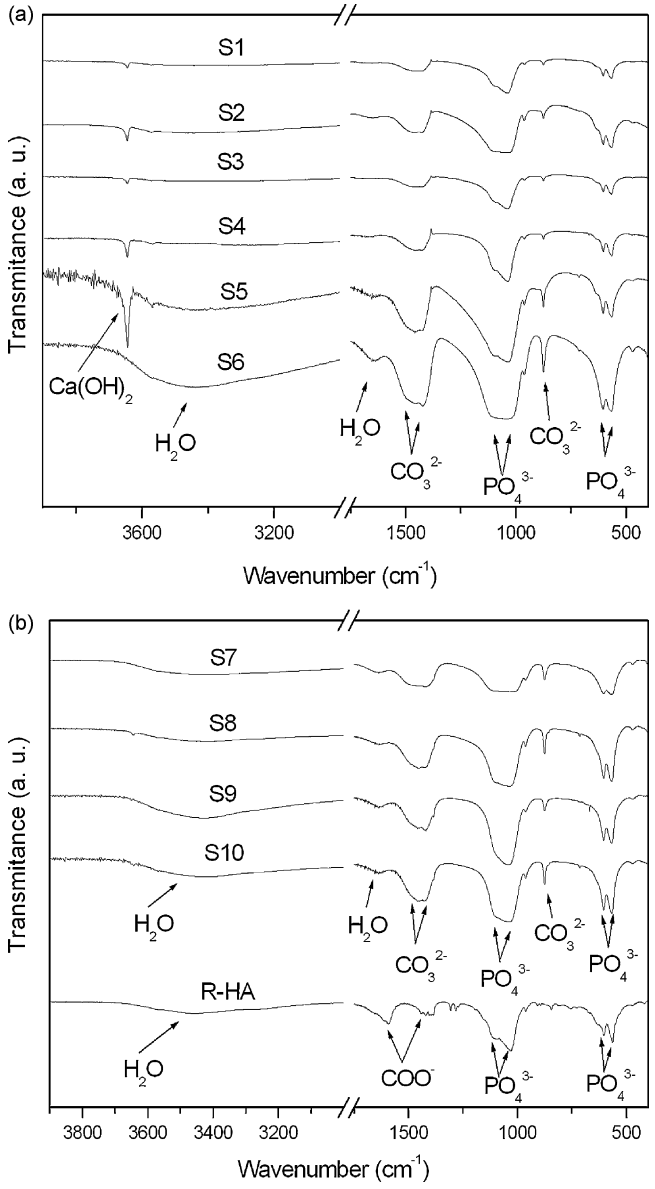

Fig. 4. FTIR of the synthesised powders. (a) G1-Group and (b) G2-Group.

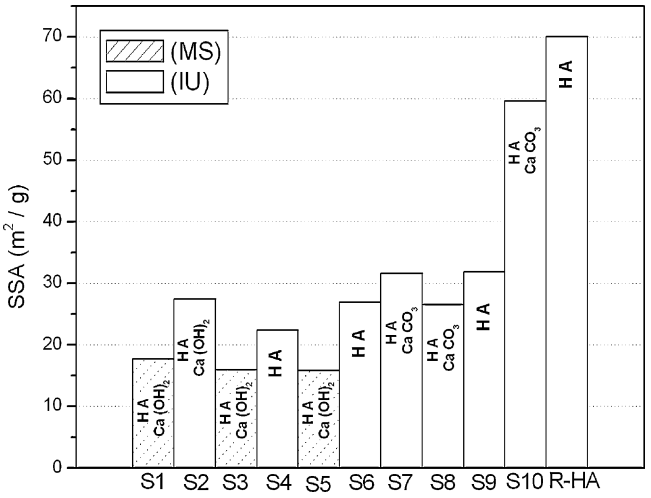

Fig. 5. SSA values determined by BET method on the synthesised powders.

and asymmetric stretch vibration at 1412 and 1596 cm^{-1} respectively) which were assigned to HA phases containing residual citrate ions. Slight bands due to CO_3^{2-} ions were detected in the R-HA spectrum [24].

The determined values of SSA (m^2/g) are plotted in Fig. 5. The values are about 20–30 m^2/g, except the one of the S10 sample. This powder, which contains HA and $CaCO_3$, showed a SSA of ~60 m^2/g, exhibiting the major value with respect to the other values obtained for synthesised samples although the S10 sample showed a crystal size similar to S9, S8, S7. However, the difference in SSA values between these samples was attributed to a different powder morphology. The dissolution–precipitation events during the ageing stage caused the formation of nanocrystals with minor compaction with respect to other synthesised powders. This is due to the low amount of matter participating in the synthesis. Consequently, the low concentration of Ca^{2+} ions in the suspension does not favour the crystal growth. The micrographs of final powders are shown in Figs. 6 and 7. By comparing the micrographs of the obtained powders by MS or UI treatment (Fig. 6), it can be shown that UI-synthesised powders possess improved morphologic features with respect to MS-obtained powders. The S2, S4 and S6 powders present reduced and uniform particle sizes when compared to S1, S3 and S5. In Fig. 7 the differences in the surfaces of S7, S8, S9 and S10 become clear compared to R-HA as reference material. The pictures revealed that S7, S8, S9 and S10 are formed by micrometric particles coated by HA nanocrystals, being the morphologic feature that provides larger values of SSA to these powders than the ones obtained for G1-samples. The shape and size of the S9-powder crystals are more similar to the R-HA than of all other samples. However, the nanocrystals in S9 are observed to be fused, which indicates that they possess minor SSA than the R-HA powder.

Choi et al. [30] discussed the specific surface area values in HA nanocrystals. They support the idea that SSA does not have any relation to the Ca/P molar ratio of HA, rather being ascribed to the relatively smaller particle sizes. This assumption is supported by the SSA value of S10 showing the smallest crystal sizes. However, it is not possible to ensure that this material (S10) is formed by isolated nanoparticles as in the R-HA.

The thermal stability was studied on samples synthesised using UI and ageing time (S6, S7, S8, S9 and S10). The obtained results were compared with the thermal stability of R-HA powder. Fig. 8 shows the typical TGA curves where the amount of mass loss is plotted against the temperature for S6, S9, S10 and R-HA. Thermogravimetric analysis showed poor thermal stability for R-HA and revealed the presence of $CaCO_3$ in the S10 sample, while S9 and S6 presented a HA structure thermally more stable. The Ca/P molar ratio of HA powder is one of the most crucial parameters in determining properties and thermal stability. It is widely known that when Ca-deficient hydroxyapatite is calcined above 700–800 °C it transforms into

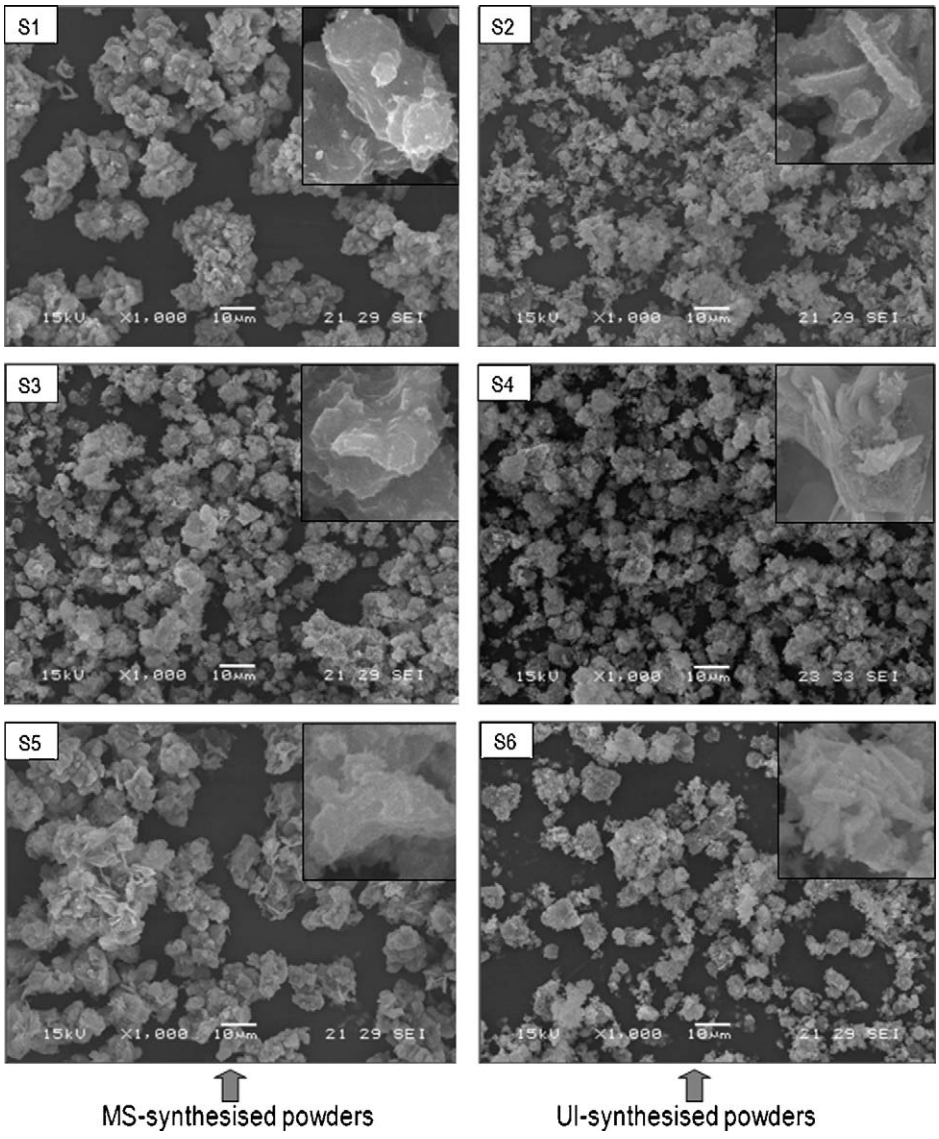

Fig. 6. SEM micrographs of the S1, S2, S3, S4, S5 and S6 synthesised powders.

β-$Ca_3(PO_4)_2$ (β-TCP) and stoichiometric HA (Ca/P = 1.67) [31,32].

The XRD spectra of the thermally treated samples show that the HA phase in the synthesised samples is stable up to 1100 °C (Fig. 9). This fact gives clear evidence that the precipitated HA phase has a stoichiometric molar Ca/P ratio. Small peak at $2\theta = 37.5$ in the XRD spectra was assigned to the CaO phase. The presence of CaO can be ascribed to the thermal decomposition of $CaCO_3$. Since the presence of CaO is not desirable, it can be eliminated washing the precipitates before the drying step.

Fig. 10 shows the crystal size (d_c) of the powders in function of the temperature of thermal treatment. At 200 °C the d_c values were similar for all UI-powders (∼50 nm). However, the R-HA showed the highest value (∼130 nm). This d_c value for R-HA was associated to the high surface energy of this material, favouring the crystal growth at low temperatures. The crystal growth for R-HA powder was sustained in the analysed temperature range. At 600 °C the crystal growth for UI-samples was relevant (∼130 nm) with respect to initial values, but resulting reduced values respect to R-HA (∼250 nm). Thermal treatment at 1100° C led to different d_c values for UI-samples, the more distinguished value resulted for S10 (that contains $CaCO_3$ as second phase). The UI-powders showed a retarded crystal growth in comparison with the reference material, maintaining reduced values of crystal size. This fact could be associated with the formation of a stoichiometric HA phase (Ca/P = 1.67) in the UI-samples, being thermally more stable than the non-stoichiometric HA phase in R-HA (Ca/P < 1.67). From the analysis of the thermal evolution of the crystal size, it is possible to conclude that the reference material showed reduced thermal stability in comparison with the UI-powders. This difference was associated to the reactivity of the powders and the specific surface area, both related to the Ca/P molar ratio.

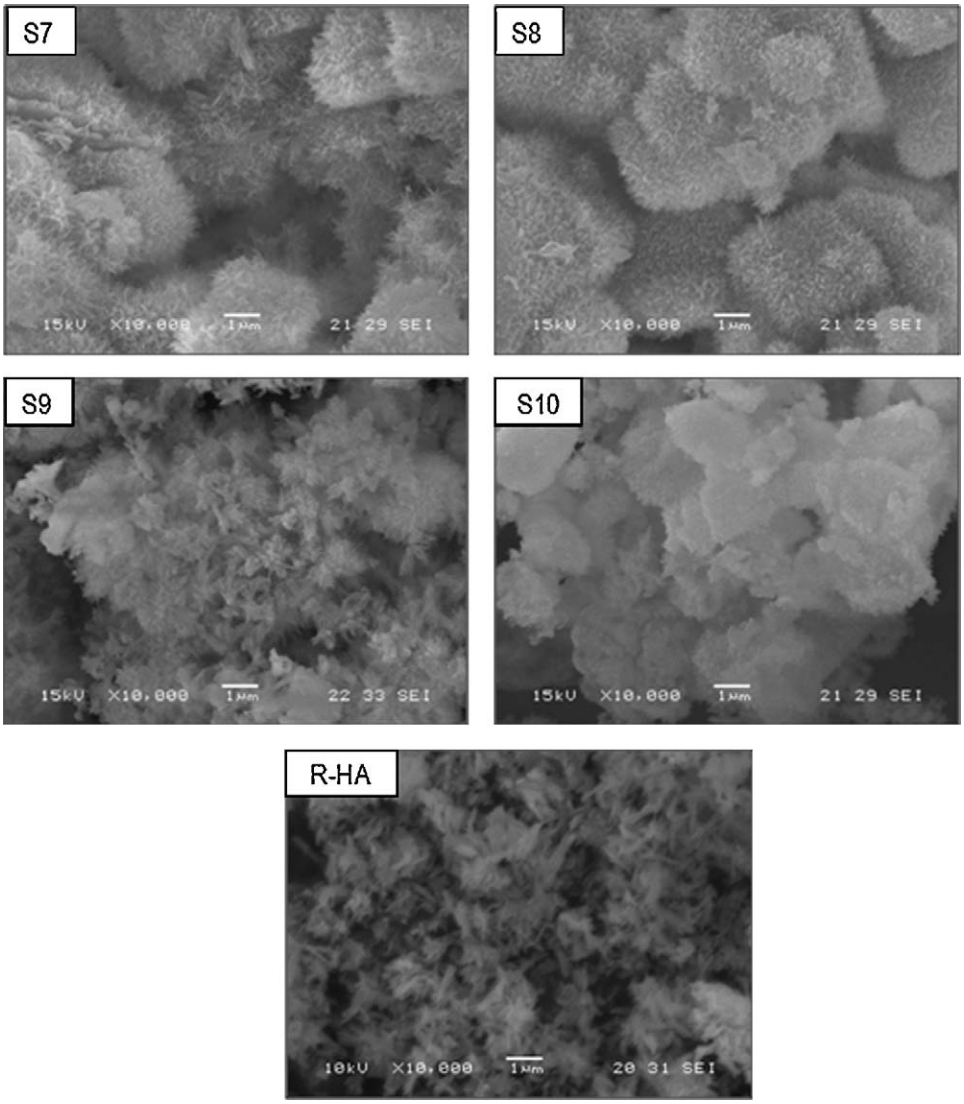

Fig. 7. SEM micrographs of the S7, S8, S9, S10 and R-HA synthesised powders.

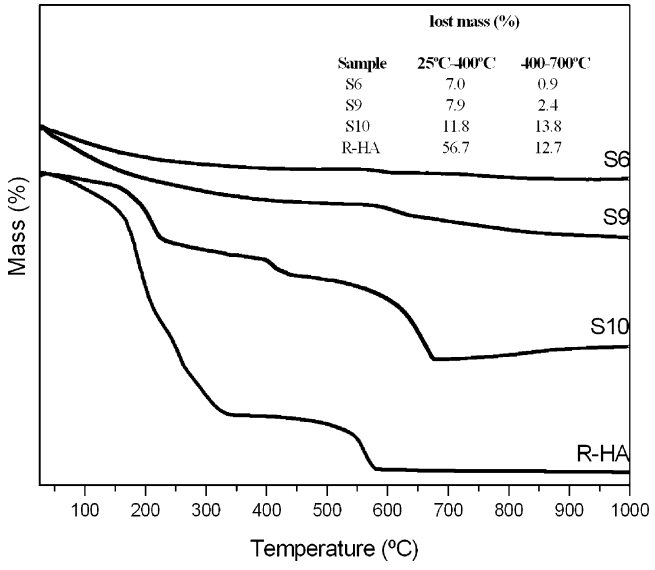

Fig. 8. TGA curves of samples S6, S9, S10 and R-HA.

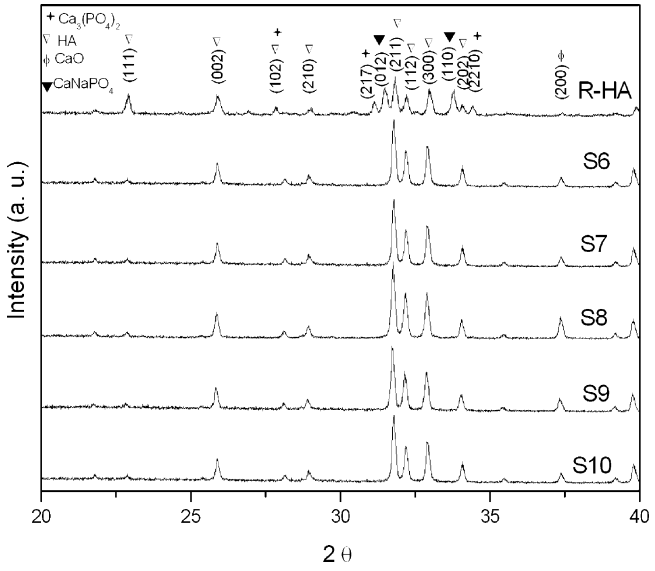

Fig. 9. XRD spectra of thermally treated samples.

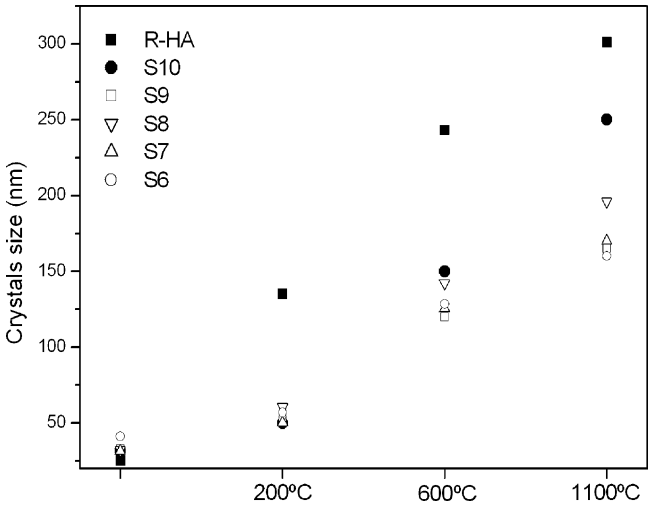

Fig. 10. Crystal size of the powders in function of treatment temperature.

4. Conclusions

An extended surface area gained by the nanosize of their constitutive crystals is crucial for biomedical applications since numerous functions of the bone mineral evolve at the interface between the surface of such apatite nanocrystals and the surrounding biological fluids. This study revealed the feasibility to produce HA powders with controlled crystal size between 31.7 and 70.6 nm by an ultrasonic assisted precipitation method. HA powder with similar surface area as the reference HA can be obtained adjusting experimental conditions. The high power of UI employed in the synthesis favoured the formation of pure HA phase. The used method allowed us to synthesise HA powders with thermal stability up to 1100 °C.

Acknowledgements

Authors would like to thank the financial support of the following institutions: National Research Council (CONICET, Argentina), National Agency for the Promotion of Science and Technology (ANPCyT, Argentina) and University of Mar del Plata (Argentina).

References

[1] Hydroxyapatite and Related Materials. Boca Raton, FL, USA: CRC Press, Inc.; 1994. ISBN 0-8493r-r4750-5.
[2] K.P. Sanosh, M.C.H. Chu, A. Balakrishnan, Y.J. Lee, T.N. Kim, S.J. Cho, Synthesis of nano hydroxyapatite powder that simulate teeth particle morphology and composition, Current Applied Physics 9 (6) (2009) 1459–1462.
[3] J.R. Jones, New trends in bioactive scaffolds: the importance of nanostructure, Journal of the European Ceramic Society 29 (7) (2009) 1275–1281.
[4] S.J. Kalita, A. Bhardwaj, H.A. Bhatt, Nanocrystalline calcium phosphate ceramics in biomedical engineering, Materials Science and Engineering: C 27 (3) (2007) 441–449.
[5] Vasiliev, E. Zlotnikov, J.G. Khinast, R.E. Riman, Chemisorption of silane compounds on hydroxyapatites of various morphologies, Scripta Materialia 58 (12) (2008) 1039–1042.
[6] H.J. Lee, H.W. Choi, K.J. Kim, H. Kim, S.C. Lee, Modification of hydroxyapatite nanosurfaces for enhanced colloidal stability and improved interfacial adhesion in nanocomposites, Chemistry of Materials 18 (2006) 5111–5118.
[7] S.J. Segvich, H.C. Smith, D.H. Kohn, The adsorption of preferential binding peptides to apatite-based materials, Biomaterials 30 (7) (2009) 1287–1298.
[8] I. Mobasherpour, M.S. Heshajin, A. Kazemzadeh, M. Zakeri, Synthesis of nanocrystalline hydroxyapatite by using precipitation method, Journal of Alloys and Compounds 430 (1–2) (2007) 330–333.
[9] H. Eshtiagh-Hosseini, M.R. Housaindokht, M. Chahkandi, Effects of parameters of sol–gel process on the phase evolution of sol–gel-derived hydroxyapatite, Materials Chemistry and Physics 106 (2–3) (2007) 310–316.
[10] M. Toriyama, A. Ravaglioli, A. Krajewski, G. Celotti, A. Piancastelli, Synthesis of hydroxyapatite-based powders by mechano-chemical method and their sintering, Journal of the European Ceramic Society 16 (4) (1996) 429–436.
[11] V. Jokanovic, D. Izvonar, D. Dramicanin, B. Jokanovic, V. Zivojinovic, D. Markovic, B. Dacic, Hydrothermal synthesis and nanostructure of carbonated calcium hydroxyapatite, Journal of Materials Science: Materials in Medicine 17 (6) (2006) 539–546.
[12] S. Yamaguchi, T. Yabutsuka, M. Hibino, T. Yao, Generation of hydroxyapatite patterns by electrophoretic deposition, Journal of Materials Science: Materials in Medicine 19 (3) (2007) 1419–1424.
[13] C. Li, The crystallinity of calcium phosphate powders influenced by the conditions of neutralized procedure with citric acid additions, Materials Research Bulletin 44 (5) (2009) 1136–1141.
[14] X. Guo, P. Xiao, Effects of solvents on properties of nanocrystalline hydroxyapatite produced from hydrothermal process, Journal of the European Ceramic Society 26 (15) (2006) 3383–3391.
[15] I. Smičiklas, A. Onjia, S. Raičević, Experimental design approach in the synthesis of hydroxyapatite by neutralization method, Separation and Purification Technology 44 (2) (2005) 97–102.
[16] S. Madhavi, C. Ferraris, T.J. White, Synthesis and crystallization of macroporous hydroxyapatite, Journal of Solid State Chemistry 178 (9) (2005) 2838–2845.
[17] B. Viswanath, N. Ravishankar, Controlled synthesis of plate-shaped hydroxyapatite and implications for the morphology of the apatite phase in bone, Biomaterials 29 (36) (2008) 4855–4863.
[18] S.C.J. Loo, Y.E. Siew, S. Ho, F.Y.C. Boey, J. Ma, Synthesis and hydrothermal treatment of nanostructured hydroxyapatite of controllable sizes, Journal of Materials Science: Materials in Medicine 19 (3) (2007) 1389–1397.
[19] L.Y. Cao, Ch.B. Zhang, J.F. Huang, Synthesis of hydroxyapatite nanoparticles in ultrasonic precipitation, Ceramics International 31 (8) (2005) 1041–1044.
[20] D.J. Gupta, S. Venugopal, V.R. Mitra, D. Giri, S. Ramakrishna, Nanostructured biocomposite substrates by electrospinning and electrospraying for the mineralization of osteoblasts, Biomaterials 30 (2009) 2085–2094.
[21] A. Gedanken, Using sonochemistry for the fabrication of nanomaterials, Ultrasonics Sonochemistry 11 (2) (2004) 47–55.
[22] M. Campos, F.A. Müller, A.H.A. Bressiani, J.C. Bressiani, P. Greil, Sonochemical syntesis of calcium phosphate powders, Journal of Materials Science: Materials in Medicine 18 (2007) 669–675.
[23] Y. Han, S. Li, X. Wang, I. Bauer, M. Yin, Sonochemical preparation of hydroxyapatite nanoparticles stabilized by glycosaminoglycans, Ultrasonics Sonochemistry 14 (3) (2007) 286–290.
[24] A. López-Macipe, J. Gómez-Morals, R. Rodriguez-Clemente, Hydroxyapatite nanoparticles precipitation from homogeneous Ca–citrate complexed aqueous solutions using microwaves and conventional heating, Advanced Materials 10 (1998) 19–53.
[25] W. Kim, F. Saito, Sonochemical synthesis of hydroxyapatite from H_3PO_4 solution with $Ca(OH)_2$, Ultrasonics Sonochemistry 8 (2) (2001) 85–88.
[26] M.G. Taylor, S.F. Parker, P.C.H. Mitchell, A study by high energy transfer inelastic neutron scattering spectroscopy of the mineral fraction of ox femur bone, Journal of Molecular Structure 651–653 (2003) 123–126.

[27] A. Nanni, L. Dei, $Ca(OH)_2$ nanoparticles from W/O microemulsions, Langmuir 19 (2003) 933–938.
[28] A.M. Kalinkin, E.V. Kalinkina, O.A. Zalkind, T.I. Makarova, Chemical interaction of calcium oxide and calcium hydroxide with CO_2 during mechanical activation, Inorganic Materials 41 (2005) 1073–1079.
[29] E. Fleet, Infrared spectra of carbonate apatites: ν_2-region bands, Biomaterials 30 (8) (2009) 1473–1481.
[30] H.W. Choi, H.J. Lee, K.J. Kim, H. Kim, S.C. Lee, Surface modification of hydroxyapatite nanocrystals by grafting polymers containing phosphonic acid groups, Journal of Colloid and Interface Science 304 (1) (2006) 277–281.
[31] N.Y. Mostafa, Characterization, thermal stability and sintering of hydroxyapatite powders prepared by different routes, Materials Chemistry and Physics 94 (2–3) (2005) 333–341.
[32] Y.X. Pang, X. Bao, Influence of temperature, ripening time and calcination on the morphology and crystallinity of hydroxyapatite nanoparticles, Journal of the European Ceramic Society 23 (10) (2003) 1697–1704.